Journal of Hazardous Materials 186 (2011) 1601–1614

Contents lists available at ScienceDirect

Journal of Hazardous Materials

journal homepage: www.elsevier.com/locate/jhazmat

# Experimental investigation and numerical modeling of light nonaqueous phase liquid dissolution and transport in a saturated zone of the soil

Abbas H. Sulaymon, Hatem Asal Gzar*

*Environmental Engineering Department, College of Engineering, University of Baghdad, Al-Jadria, Baghdad, Iraq*

ARTICLE INFO

*Article history:*
Received 15 June 2010
Received in revised form
15 November 2010
Accepted 9 December 2010
Available online 15 December 2010

*Keywords:*
Light nonaqueous phase liquid
Saturated porous media
Dissolution
Mass transfer
Measurements
Numerical modeling

ABSTRACT

The present research aims at studying the dissolution and transport process of benzene as a light nonaqueous phase liquid (LNAPL) in saturated porous media. This process is studied under unidirectional flow at different water velocities ranging from 0.90 to 3.60 cm/h in a three-dimensional saturated sand tank (100 cm × 40 cm × 35 cm). This tank represents a laboratory-scale aquifer. The dispersion parameters of the sand tank are based on an independent tracer experiments. The experimental aquifer is simulated by developing a three-dimensional finite element numerical model. This model assumes that the dissolved concentration along the LNAPL–water interface is equal to the solubility concentration. The numerical model results overpredict the experimental within factor 1.6 and 2.29 at depths of 1 cm and 3 cm, respectively, during eight days. The correlation coefficient is ranging from 0.8485 to 0.9986. The time invariant average mass transfer coefficient is determined at each interstitial velocity. The values are ranged from 0.016 to 0.061 cm/h (i.e. increased with velocity toward a limiting value). For a circular benzene pool, two linear relationships are found; the first between the overall Sherwood number ($Sh^*_{(e)}$) with average Peclet number in $x$-direction ($Pe^*_{x(e)}$); and the second between the overall Sherwood number ($Sh^*_{(e)}$) with average Peclet number in $y$-direction ($Pe^*_{y(e)}$).



## 1. Introduction

The contamination of soil and ground-water by petroleum hydrocarbons has been a major concern of many studies during the last two decades. The most frequent cause of contamination is leakage from underground storage tanks, pipelines, spillages from overfilling or accidents during transferring fuel [1]. When pollution occurs, a number of dangerous substances migrate through ground-water then enter into food and water chain. Finally, directly or indirectly harm human [2,3].

Nonaqueous phase liquids are hydrocarbons that exist as a separate and immiscible phase, when they contact with water and/or air. Difference in the physical and chemical properties of water and nonaqueous phase liquid (NAPL) resulted in the formation of a physical interface between the liquids which prevents the two fluids from mixing. Nonaqueous phase liquids are typically classified into two kinds: first, light nonaqueous phase liquids (LNAPLs) which have densities less than that of water; second, dense nonaqueous phase liquids (DNAPLs) which have densities greater than that of water. The most common LNAPLs related ground-water contamination problems are resulted from the release of petroleum products. These products are typically multicomponent organic mixture composed of chemicals with varying degrees of water solubility. Examples of LNAPLs include gasoline are jet fuel and heating oils. Gasoline is made up of mono-aromatic compounds such as benzene, toluene, ethylbenzene, and xylenes (including ortho-xylenes, meta-xylenes, and para-xylenes), which are collectively called BTEX compounds. These compounds make up about 18% by weight of gasoline. The effective solubilities of BTEX compounds are lower than their single-compound aqueous solubilities. BTEX represent potential long-term sources for continued ground-water contamination at many sites [4,5].

When the BTEX compounds enter water or food chain, they can be fatal for human life, causing harm in short or long term. In particular, benzene, which is considered as carcinogenic and mutagenic as well as a major pollutant according to the Environmental Protection Agency (EPA) and National Primary Drinking Standards [3,6].

In physical contact with ground-water, a NAPL will dissolve into the aqueous phase. The solubility of an organic compound is the equilibrium concentration of the compound in water at a specified temperature and pressure. For all practical purposes, the solubility represents the maximum concentration of that compound in water [4].

The aqueous-phase concentrations of dissolved NAPLs in ground-water are primarily governed by interphase mass transfer processes which are often slow and rate-limited [7].

* Corresponding author.
*E-mail address:* hatam_asal@yahoo.com (H.A. Gzar).

0304-3894/$ – see front matter © 2011 Elsevier B.V. All rights reserved.
doi:10.1016/j.jhazmat.2010.12.035

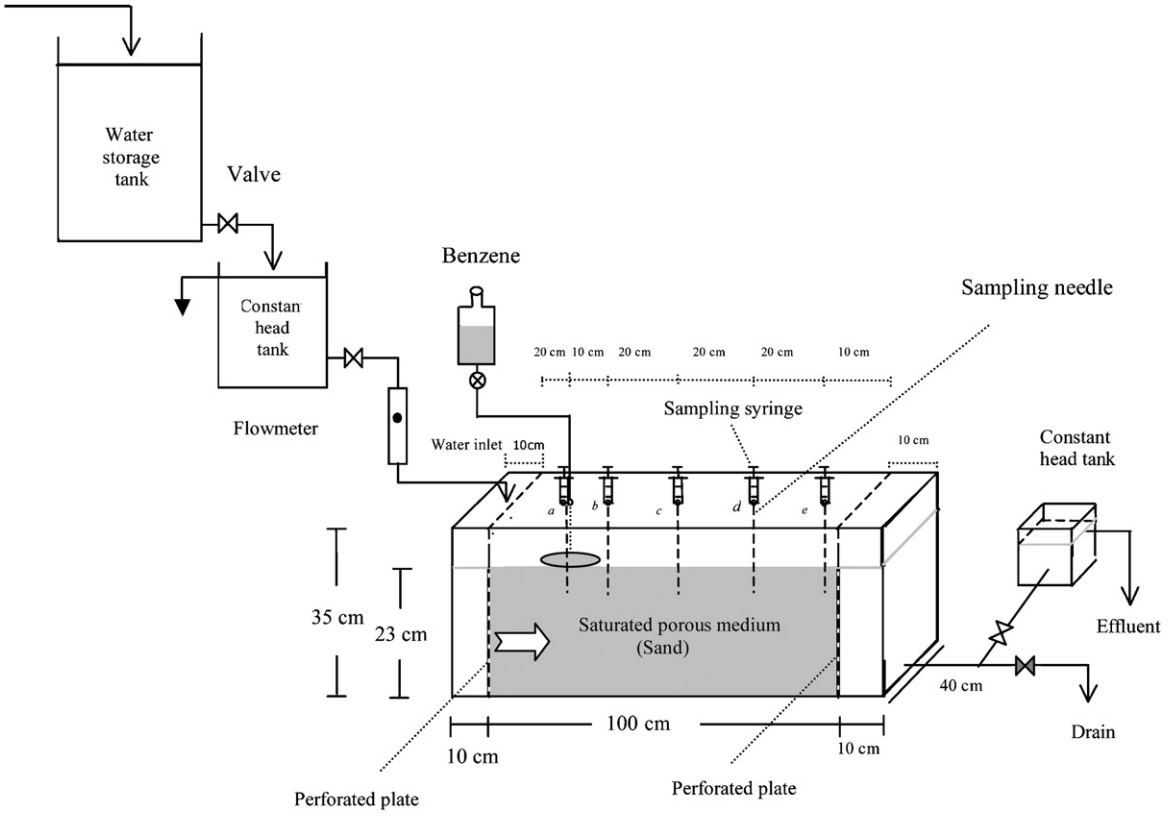


**Fig. 1.** A schematic diagram of the laboratory-scale aquifer (three-dimensional sand tank, 100 cm × 40 cm × 35 cm).

Only a limited number of experimental studies have focused on characterizing the NAPL dissolution process under three-dimensional flow conditions [8–14]. These studies have demonstrated the importance of three-dimensional experiments and also emphasized the need for integrating NAPL dissolution models within contaminant transport modeling framework.

The objective of the present paper is to find the dissolution and transport of benzene as a LNAPL in three-dimensional homogeneous, isotropic, and saturated porous media. For this purpose a numerical model is developed to simulate the dissolution and transport of LNAPL through three-dimensional homogeneous, isotropic, and saturated porous media. This numerical model solves the three-dimensional transport equation.

## 2. Experimental design

### 2.1. Design of the experimental aquifer

The tracer transport and dissolution experiments are conducted in a three-dimensional intermediate-scale sand tank model. The tank is made of 1 cm thick Perspex plates with dimensions of 120 cm long by 40 cm wide by 35 cm high. Two perforated Perspex plates are used. Each one is located 10 cm away from both sides dividing the tank into three chambers. The middle chamber is filled with saturated porous sand, and the chambers at both sides are filled with water to maintain constant heads. A filtration cloth is fixed on the perforated plates to prevent passing the sand into the chambers at both sides of the aquifer. Fig. 1 shows a schematic diagram of the aquifer model and the auxiliary equipments. The auxiliary equipments consist of 125 l storage tank contains tap water, two constant head reservoirs of 20 l and 3 l volumes, respectively, and a flowmeter (Cole-Parmer Instrument Co., Chicago, IL, USA) [15].

### 2.2. LNAPL pool formation and aquifer packing

A circular plastic bowl of 15 cm inner diameter and 5 cm height is used to confine the LNAPL (benzene) pool at the surface of the experimental aquifer. The aquifer tank is filled with sand to a height 23 cm and the water covers all the sand. The bowl is inversely placed on the upper surface of the water-saturated sand, so the open side of the bowl directly faced the sand. The aim of this configuration is to keep the pool within 15 cm of the porous media. The bowl is fixed by four screws with the Perspex cover of tank (Fig. 1). The LNAPL is dyed with Sudan III which is a powdered, nonvolatile organic dye of red color, soluble in hydrocarbons and insoluble in water. The red dye is added to assist the visual observation of the LNAPL pool. The thickness of the floating LNAPL pool in the bowl is 1 cm. The pool is injected at a rate of 18 ml/h.

Sand is used as a porous medium. The properties of this sand are measured. 1 mm sand packed into tank to height of 23 cm. This configuration results in a packed volume of about 92,000 $cm^3$ (100 cm × 40 cm × 23 cm). The tank is filled with water and left overnight to settle and saturate the sand. The system is then flushed at maximum velocity until the effluent water is free of suspended fine material. After each experiment, the used sand is removed from the tank. The tank is washed and cleaned very well and then filled with new sand for a new experiment.

A small stream of 200 mg/l sodium azide solution is introduced to the influent water at the chamber in the left side of aquifer to inhibit biological growth [16].

### 2.3. Dissolution experiments

Five sampling ports (*a–e*) are made in the Perspex cover of sand tank. The samples withdraw from ten sampling points. Five of them at 1 cm depth, and the other five are at 3 cm depth. All sam-

pling points located in the centerline of the aquifer (at $y = 20$ cm) in order to study the longitudinal distribution of concentration with distance, at two depths. Also, the maximum concentrations of pollutant occur in the centerline of plume. The more dispersion is occurred in the longitudinal or horizontal direction (in the direction of flow) compared with the transverse and vertical directions. The experiments are conducted at five different interstitial velocities.

For collecting samples, 15-gauged stainless-steel needles (manufactured by Sherwood Medical, St. Louis, MO, USA) are inserted into the ports and pushed into the porous medium. Wire is inserted inside the needle during the placement process to prevent clogging.

Ten dissolution experiments are conducted in the three-dimensional bench scale aquifer. These experiments are divided into two sets of samples; each one is collected from five selected points within the aquifer downstream from the LNAPL pool at a selected interstitial velocity. The first set is at depth $z = 1$ cm. The sampling points located at (−7.5, 20, 1), (2.5, 20, 1), (22.5, 20, 1), (42.5, 20, 1), and (62.5, 20, 1), respectively. The second set of the samples is at depth $z = 3$ cm. The sampling points located at (−7.5, 20, 3), (2.5, 20, 3), (22.5, 20, 3), (42.5, 20, 3), and (62.5, 20, 3), respectively. The points (−7.5, 20, 1) and (−7.5, 20, 3) refer to the sampling points below the LNAPL pool at depths of 1 cm and 3 cm, respectively. Five interstitial velocities of 0.90, 1.80, 2.34, 2.70, and 3.60 cm/h are used.

The flow of water from the storage tank and the constant head tank is transferred by gravity. The water elevation in the aquifer is maintained at the desired level by using two constant head reservoirs; one before the inlet and the other after the outlet of the aquifer. A flowmeter is used to measure the water flow rate from the constant head tank to the aquifer. The flowrate is ranged from 5 to 20 ml/min. These flowrates yield an interstitial velocity of 0.90–3.60 cm/h. All experiments are conducted at temperature of $20 \pm 1\,^{\circ}$C.

### 2.4. Sample collection and analysis

Aqueous phase LNAPL is collected only when steady-state concentrations are observed at sampling port ($e$), which is the sampling port farthest away from the LNAPL pool. Interstitial water samples are collected from ports of the sand tank using syringe-needles (Fig. 1). The volume of the used syringe is 5 ml. A 1 ml of sample is withdrawn from each location and stored in a glass vial, sealed with Teflon-lined septa. The number of collected samples from the five ports in the porous medium is 200 samples at the depth of 1 cm and other 200 samples are at depth of 3 cm from the top. The samples are analyzed using gas chromatograph equipped with flame ionization detector (Gas Chromatograph GC-2014, Shimadzu Corporation, Analytical & Measuring Instrument Division, Kyoto, Japan).

### 2.5. Tracer analysis

The tracer transport test is the most common system used for determining the dispersion coefficients, using brine solution as tracer, the concentration of the tracer is determined by using conductivity and resistivity meters [17–21]. A tracer transport experiments are performed to find the longitudinal dispersion coefficients values of the sand in the tank. A solution of tap water and sodium chloride with an initial concentration of 1000 mg/l is used.

The tracer test is conducted by continuously injecting sodium chloride solution with different water velocities of 0.90, 1.80, 2.34, 2.70, and 3.60 cm/h. The injection rate is fixed at a constant flowrate of 20 ml/min. The breakthrough data is continuously recorded at observation point located at 40 cm from the injected tracer. The concentration measurements are done by using portable ohmmeter probe. This probe is placed from the top of the tank, in the observation point at depth of 3 cm in the saturated porous medium. The ohmmeter probe measures the resistance (hence the concentration variations) of diluted sodium chloride tracer. The measured resistance is calibrated by using samples of known concentrations. For this purpose, a calibrated curve is prepared. The experiments are carried out to record the breakthrough at interstitial velocities of 0.90, 1.80, 2.34, 2.70, and 3.60 cm/h as shown in Fig. 2.

## 3. Transport model

The transient contaminant transport from a dissolving NAPL pool in a three-dimensional homogeneous porous medium under steady state uniform flow conditions; for non-decaying dissolved organic and if sorption occurs under local equilibrium conditions; is governed by [15,22,23]:

$$D_x \frac{\partial^2 C(t,x,y,z)}{\partial x^2} + D_y \frac{\partial^2 C(t,x,y,z)}{\partial y^2} + D_z \frac{\partial^2 C(t,x,y,z)}{\partial z^2} - V_x \frac{\partial C(t,x,y,z)}{\partial x} = R_f \frac{\partial C(t,x,y,z)}{\partial t} \quad (1)$$

where $V_x$ is the average unidirectional interstitial ground water velocity; $R_f$ is the dimensionless retardation factor; and $D_x$, $D_y$, and $D_z$ are the longitudinal, transverse, and vertical hydrodynamic dispersion coefficients, respectively.

The initial and boundary conditions for a circular-shaped stagnant LNAPL pool as shown in Fig. 3 are:

$$C(0,x,y,z) = 0 \quad (2)$$

$$C(t,\pm\infty,y,z) = 0 \quad (3)$$

$$C(t,x,\pm\infty,z) = 0 \quad (4)$$

$$C(t,x,y,0) = C_s, \quad x,y \in R_{(e)} \quad (5)$$

$$\frac{\partial C(t,x,y,0)}{\partial z} = 0, \quad x,y \notin R_{(e)} \quad (6)$$

$$C(t,x,y,\infty) = 0 \quad (7)$$

where $C_s$ is the solubility concentration of the LNAPL (for benzene $C_s$ is 1770 mg/l) and $R_{(e)}$ is the circular LNAPL–water interfacial area, defined by

$$(x - l_{xo})^2/r^2 + (y - l_{yo})^2/r^2 \leq 1$$

## 4. Numerical solution

The three-dimensional advection-dispersion transport equation (Eq. (1)); in saturated, homogeneous, and isotropic porous medium and for a uniform flow field; is solved numerically by finite element using Galerkin's method. A computer program, for two-dimensional advection-dispersion problem presented by [24], is developed in the present research to solve Eq. (1). The finite element computer program is written in Fortran 90 language.

The element size is 2.5 cm × 2.5 cm × 1.0 cm and the total number of elements is 14,720. The grid size is 100 cm × 40 cm × 23 cm. The input parameters values used in the programmed numerical model are shown in Table 1.

Fig. 4 illustrates the three-dimensional mesh of the laboratory-scale aquifer. The ports $a$, $b$, $c$, $d$, and $e$ are to draw the samples from different horizontal and vertical distances of the porous medium. Note that the needle enters port ($a$) and passing through the center of circular LNAPL pool to draw the samples from the porous medium at different depths below the pool.

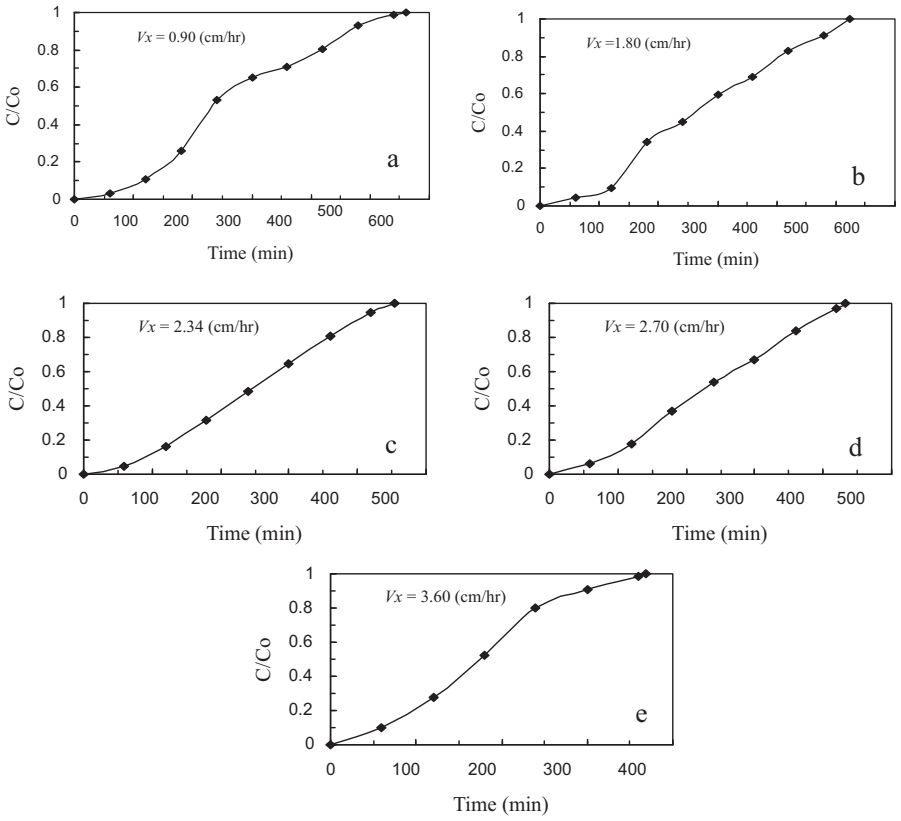


**Fig. 2.** Longitudinal breakthrough curve at velocities (a) 0.90 cm/h, (b) 1.80 cm/h, (c) 2.34 cm/h, (d) 2.70 cm/h, and (e) 3.60 cm/h.

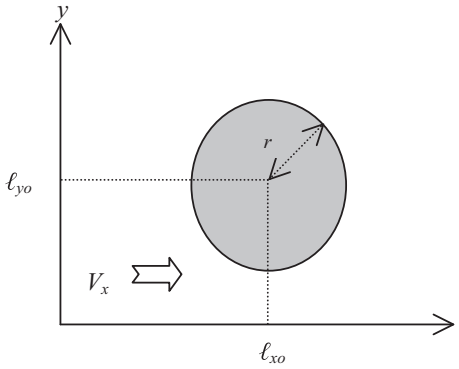


**Fig. 3.** Plan view at $z = 0$ of the circular LNAPL pool with radius $r$ and the pool center located at $x = \ell_{xo}$, $y = \ell_{yo}$. The unidirectional groundwater velocity $V_x$ and origin of the corresponding Cartesian coordinate system are shown.

**Table 1**
Numerical model input parameters values.

| Parameter | Value | Units |
|---|---|---|
| Interstitial velocity ($V_x$) | 0.90–3.60 | cm/h |
| Longitudinal dispersion coefficient ($D_x$) | $2.84 \times 10^{-1}$ to 1.014 | $cm^2/h$ |
| Lateral dispersion coefficient ($D_y$) | $2.84 \times 10^{-2}$ to $1.014 \times 10^{-1}$ | $cm^2/h$ |
| Vertical dispersion coefficient ($D_z$) | $2.84 \times 10^{-2}$ to $1.014 \times 10^{-1}$ | $cm^2/h$ |
| Bulk density of sand ($\rho_b$) | 1.6 | $g/cm^3$ |
| Porosity ($n$) | 0.345 | – |
| Retardation factor ($R_f$) | 1.31 | – |
| Solubility of benzene ($C_s$) | 1770 | mg/l |
| Time step ($\Delta t$) | 24 | h |
| Cell width along raws ($\Delta x$) | 2.5 | cm |
| Cell width along columns ($\Delta y$) | 2.5 | cm |
| Layer thickness ($\Delta z$) | 1 | cm |

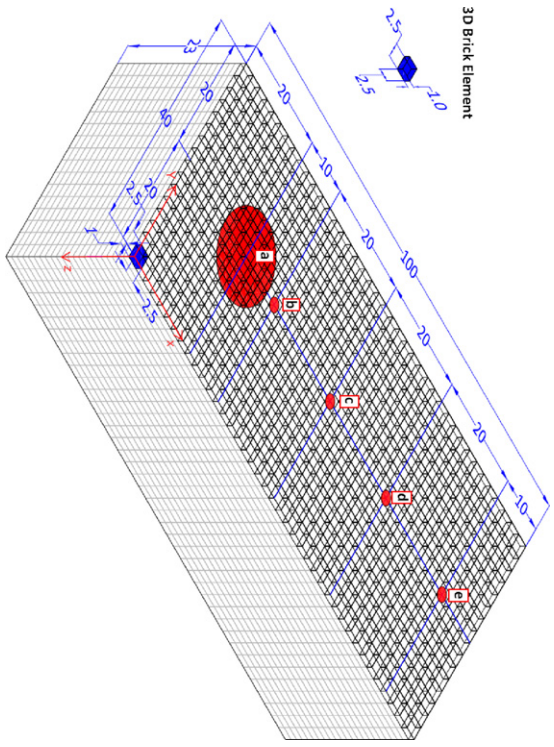


**Fig. 4.** A three-dimensional mesh of the laboratory-scale aquifer and the ports where the concentrations of LNAPL are estimated at depths ($z$): 1, 3, 6, 9, and 12 cm.

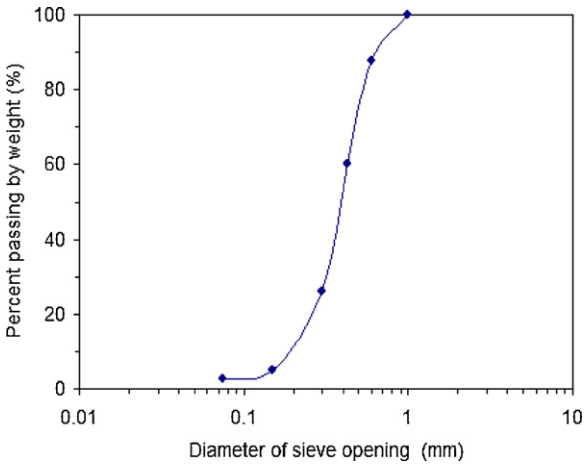


**Fig. 5.** Particle size distribution curve for the sand.

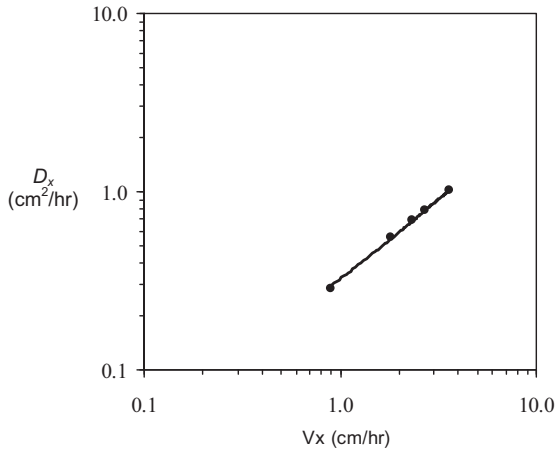


**Fig. 6.** Longitudinal dispersive curve of the tested soil.

## 5. Estimation of model parameters

### 5.1. Porous medium properties

The sand passing through 1 mm mesh is used. Samples are tested for measurement of particle size distribution by mechanical sieve analysis, porosity, as well as the permeability coefficient.

The particle size distribution is obtained by using mechanical sieve analysis as shown in Fig. 5. The uniformity coefficient ($C_u$), gives an indication of the range of grain sizes presented in a given soil sample. This coefficient is found to be 2.22 by using the following equation [25,26]:

$$C_u = \frac{D_{60}}{D_{10}} \tag{8}$$

where $D_{10}$ is the effective size and represent the grain diameter corresponding to 10% passing; $D_{60}$ is the grain diameter corresponding to 60% passing.

The porosity of the sand is determined by measuring the weight of a sample of dry sand, the weight of the saturated sample submerged in water, the volume of sample, and temperature of the water using the following equation:

$$n = \frac{v_v}{v} \tag{9}$$

$$v_v = \frac{W_s - W_d}{\rho_w} \tag{10}$$

where $n$ = porosity. $v_v$ = voids volume ($cm^3$). $v$ = total volume of sample ($cm^3$). $W_s$ = weight of the saturated water sample (g). $W_d$ = weight of the dry sample (g). $\rho_w$ = density of the water ($g/cm^3$).

The bulk density of the dry sand is 1.6 $g/cm^3$. The porosity ($n$) of the porous medium is found to be 0.345.

### 5.2. Interstitial velocity

The interstitial velocity within the model aquifer is determined by using the following equation [27]:

$$V_x = \frac{Q}{w\,h\,n} \tag{11}$$

where $Q$ is the water volumetric flowrate, $w$ is the aquifer width, $h$ is the head of water in the aquifer, and $n$ is the porosity of porous medium. Five interstitial velocities are used in the present experiments (0.90, 1.80, 2.34, 2.70, and 3.60 cm/h).

### 5.3. Hydrodynamic dispersion coefficients

The longitudinal dispersion coefficient ($D_x$) resulted from dispersive flux for each velocity is determined from tracer transport analysis experiments, using the graphical technique of relative concentration ($C/C_o$) versus time on arithmetic-probability paper. Times corresponding to ($C/C_o$) ratios of 84%, 50%, and 16% are determined and the $D_x$ is obtained from the following equation [28]:

$$D_x = 0.5\left[\frac{t_{84} - t_{16}}{2t_{50}}\right] V_x \tag{12}$$

$D_x$ found from Eq. (12) represents the longitudinal dispersion coefficient resulted from the dispersive flux. While $D_x$ obtained from diffusive flux is estimated by multiplying the coefficient of diffusion of benzene $9.8 \times 10^{-6}$ $cm^2/s$ [5] by the tortuosity of the medium. The tortuosity used for this calculation is 1.43 [29]. The final result of $D_x$ will be equal to the summation of the dispersive flux and of diffusive flux.

The vertical dispersion coefficient ($D_z$) is equal to the lateral or transverse dispersion coefficient ($D_y$) which is assumed to be 0.1 of the longitudinal dispersion coefficient ($D_y = D_z = 0.1 \times D_x$).

The values of longitudinal dispersion coefficient ($D_x$) against the corresponding values of interstitial velocity ($V_x$) are plotted on log–log scale as shown in Fig. 6. The best-fit equation is:

$$D_x = 0.2686V_x + 0.0562 \tag{13}$$

where $D_x$ in units of $cm^2/h$. In multidimensional systems, dispersion plays a critical role in determining the shape of the plume emanating from a LNAPL. Thus, accurate calculations of mass transfer coefficients for LNAPL pools require accurate dispersion parameters calculations.

### 5.4. Retardation factor

Retardation factor ($R_f$) of the sand is calculated using the following equation:

$$R_f = 1 + \frac{\rho_b}{n} K_d \tag{14}$$

where $R_f$ = retardation factor. $\rho_b$ = soil bulk density ($g/cm^3$). $n$ = porosity. $K_d$ = soil distribution coefficient.

$K_d$ describes the partitioning of a contaminant between the sorbed and bulk soil–water phases [30]. The soil distribution coefficient, $K_d$, is calculated by normalizing $K_{oc}$ for the fraction of organic carbon in the soil ($f_{oc}$):

$$K_d = K_{oc} \cdot f_{oc} \tag{15}$$

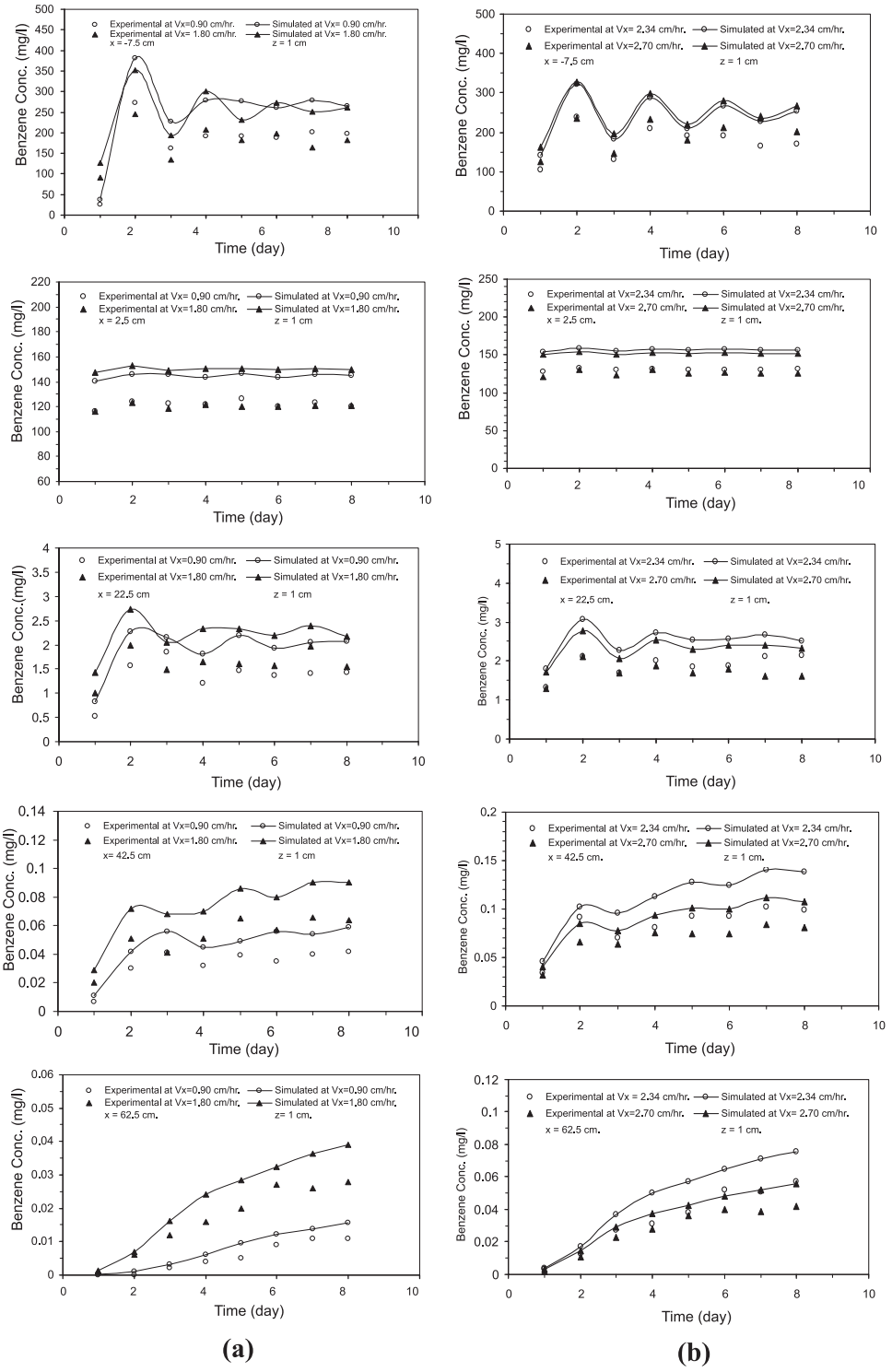


**Fig. 7.** The change of benzene concentration with time for five distances from the pool at depth ($z$) 1 cm, $y$ = 20 cm, and interstitial velocities (a) 0.90 cm/h and 1.80 cm/h; (b) 2.34 cm/h and 2.70 cm/h.

The soil adsorption coefficient, $K_{oc}$, is estimated using the regression equation (Eq. (16)) given by [31]. This equation describes the relationship between $K_{oc}$ and the octanol–water partition coefficient ($K_{ow}$) [32,33]:

$$\log K_{oc} = 0.49 + 072 \log K_{ow} \quad (16)$$

The value of $\log K_{ow}$ of the benzene is equal to 2.05 [30]. The measured carbon content of sand is 0.073% by weight. The estimated value of $R_f$ for the sand using equation (14) is 1.31.

## 6. Results and discussion

The model is used to simulate the longitudinal concentration profile at the centerline of the plume. However, local discrepancies between the model and observations are significant. These discrep-

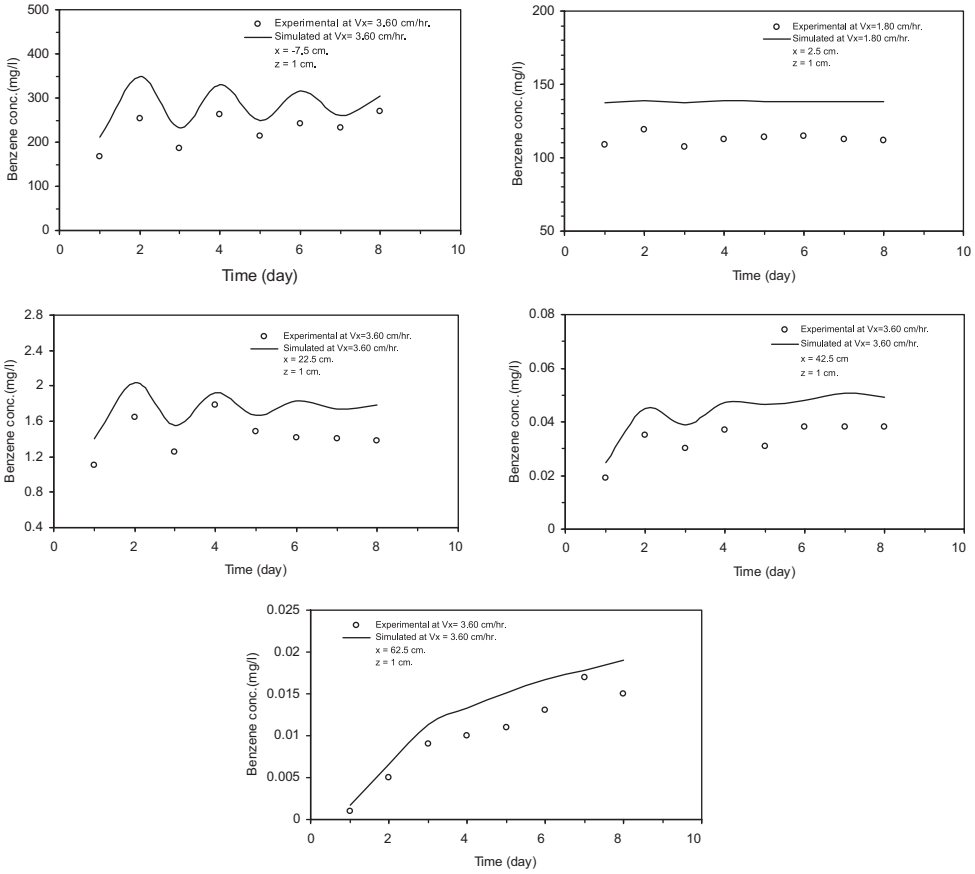


**Fig. 8.** The change of benzene concentration with time for five distances from the pool at depth ($z$) 1 cm, $y$ = 20 cm, and interstitial velocity 3.60 cm/h.

ancies may be due to the result of pore scale surface curvature and large scale shape irregularities that could not be simulated by using the present model.

The comparison between the experimental and numerical model results is carried out by using finite element grid, which represents porous medium box. Numerical simulations are completed to model the experimental data observed at the sampling points of ports *a*, *b*, *c*, *d*, and *e*.

In the finite element numerical model, LNAPL source is uniformly spread over thirty-seven grid cells, each cell have a dimensions of 2.5 cm × 2.5 cm × 1.0 cm. The total number of the grid cells of the system is 14,720 and the total number of the nodes is 16,728. The LNAPL pool volume is approximately fixed with time because the LNAPL is continuously added to the pool at a rate of 18 ml/h.

The numerical model simulations are performed to estimate profiles of aqueous phase concentration for various interstitial velocities. A zero flux boundary condition is applied to all outer boundaries of the numerical domain, and a constant boundary condition (Eq. (5)) is applied at the pool–water interface. The programmed numerical model developed in the present study is consistently run until the simulated dissolved concentration profiles are not longer time dependent, because the desired local mass transfer coefficients should correspond to steady-state conditions.

The decay rate constant is considered to be zero ($\lambda = 0$) due to the presence of sodium azide in the influent within the clear well of the model aquifer which prevents any possible biological degradation of benzene.

According to American Petroleum Institute [34], the contaminant volatilization for subsurface releases through a porous medium is usually restricted by soil moisture and fine soil texture. In the present study, the benzene pool on the water or saturated sand surface is also surrounded and covered by the plastic bowl. Accordingly, the volatilization of benzene is not considered in the numerical modeling simulations of the present study. Eq. (6) refers to that the dissolved and vapor of benzene is assumed to be zero at the surface.

In spite of the experimental results are not very close with the numerical model, but Figs. 7–10 show the same behavior of both of them with time. The numerical results are overestimated compared with the experimental ones. The reason behind that is the solubility of benzene ($C_s$) or saturation concentration (maximum concentration of benzene) of 1770 mg/l is used as an initial concentration condition in the numerical model. But in fact the value of $C_s$ in the dissolution experiments is not reached the maximum value (1770 mg/l) because the higher dissolution rates can be associated with: (1) higher interstitial velocity, (2) higher LNAPL saturation in the porous media, and (3) increased contact area between LNAPL and water.

It is noticed that the maximum value of concentration at the nearest location to the pool/water interface ($x = -7.5$, $y = 20$, $z = 1$) do not exceed the value of 272.14 mg/l through the time of experiments. Therefore the simulated concentrations are more than those of the experimental ones within factor of 1.60 for depth of 1 cm and 2.29 for depth of 3 cm in porous media.

On the other hand, the difference between the experimental and numerical results can be attributed to the fact that many variables related to the porous medium, which are assumed to be constant when the numerical solution is adopted, do not agree with the natural geometry of the sand.

Another reason for the discrepancies in experimental and numerical concentration results (Figs. 7–10) is probably due to the

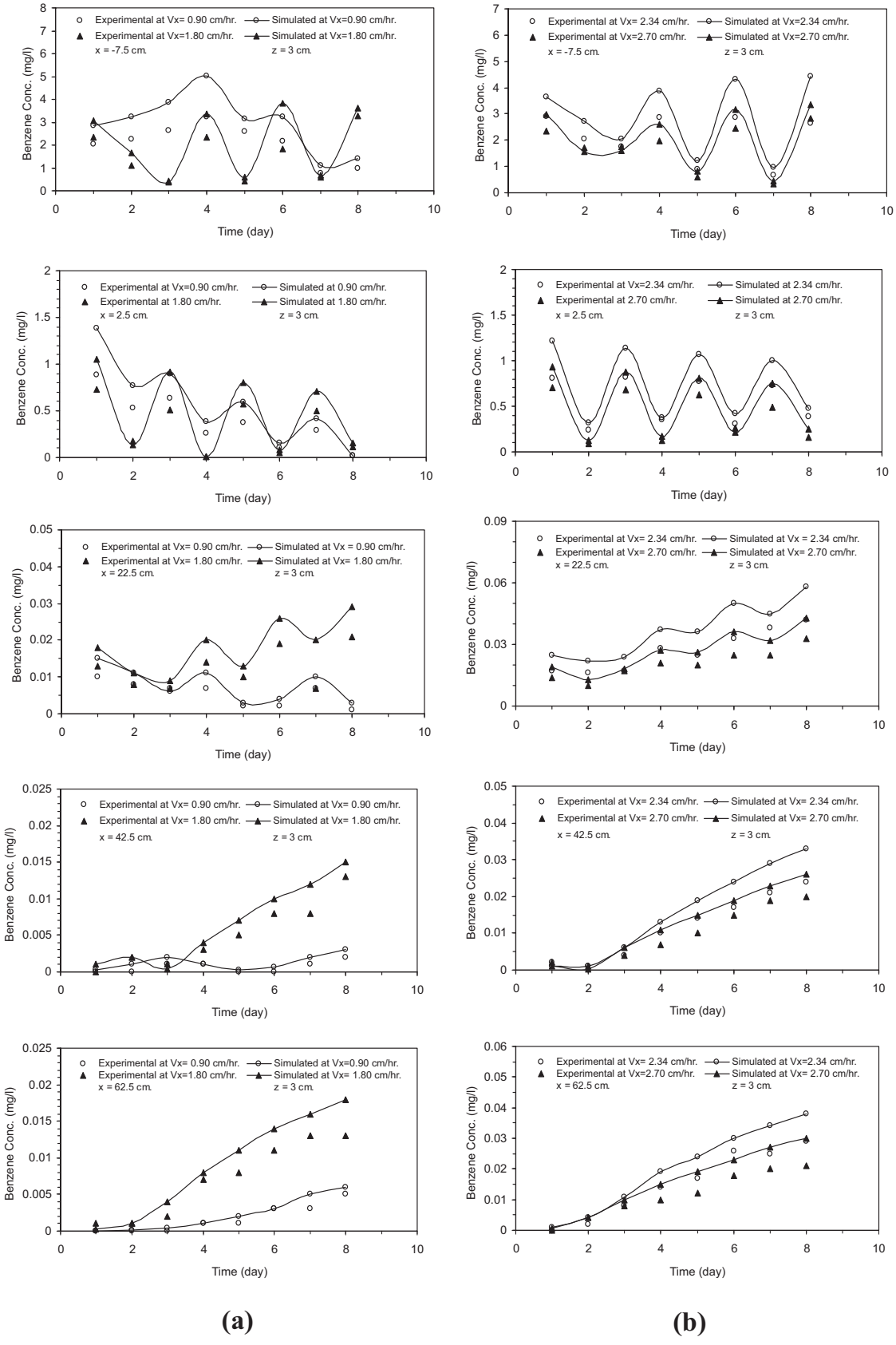


**Fig. 9.** The change of benzene concentration with time for five distances from the pool at depth ($z$) 3 cm, $y$ = 20 cm, and interstitial velocities (a) 0.90 cm/h and 1.80 cm/h; (b) 2.34 cm/h and 2.70 cm/h.

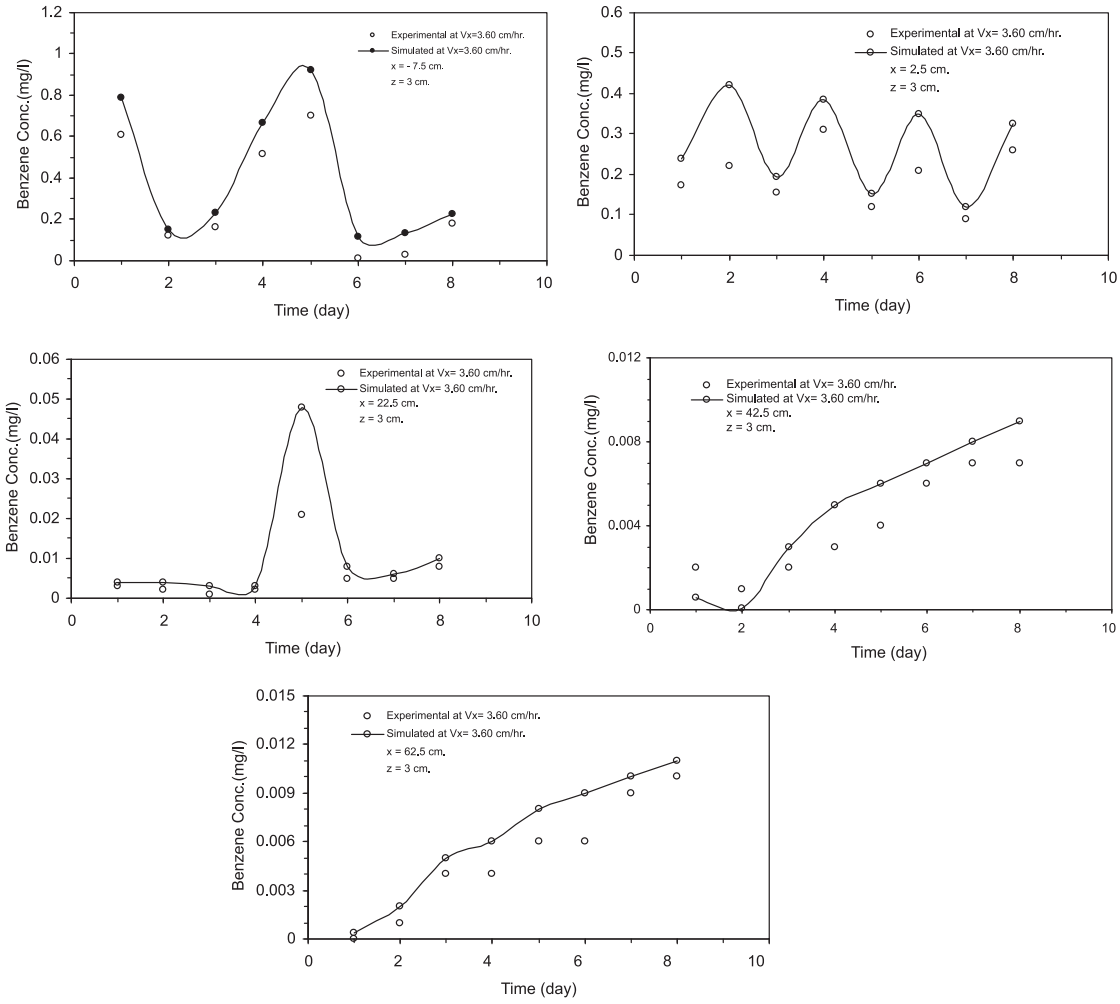


**Fig. 10.** The change of benzene concentration with time for five distances from the pool at depth ($z$) 3 cm, $y$ = 20 cm, and interstitial velocity 3.60 cm/h.

method of tracer transport analysis experiments which is used to determine the longitudinal dispersion coefficient.

At depth ($z$) 1 cm, and at the same horizontal distance ($x$), the concentration profiles with time in Fig. 7(a) approximately similar to those in Fig. 7(b). In Fig. 7(a), the concentration values increased with increasing velocity from 0.90 cm/h to 1.80 cm/h except that at distance −7.5 cm which located under the benzene pool ($x$ = −7.5 cm, $y$ = 20 cm, $z$ = 1 cm). While in Fig. 7(b) at the same horizontal distance, the concentration values decreased with increasing velocity from 2.34 cm/h to 2.70 cm/h, except that at distance −7.5 cm. It can be observed the same behavior in Fig. 8 when the velocity increased to 3.60 cm/h.

In Figs. 7–10, the concentration profiles with time when the depth $z$ equals to 3 cm are noticed to be a wave shape at distance from −7.5 cm to 22.5 cm in the aquifer at location near the source. Also at depth of 1 cm, the profiles have a wave shape are noticed at distances from −7.5 cm to 42.5 cm except at 2.5 cm. The wave behavior of experimental results may be due to the result of pore scale geometry and large scale shape irregularities (these two factors does not show dominating factors in the present research). The numerical simulation at specific interstitial velocity (consequently, constant dispersion coefficients) gives constant concentration gradient at specific time interval. As shown in Fig. 11, it is noticed at $z$ = 1 cm and time 8 days, the concentration at $x$ = 2.5 cm is 138–157 mg/l and at $x$ = 62.5 cm is 0.016–0.076 mg/l for all values of interstitial velocity. For this simulation, the driving force for the accumulation of benzene at specific locations at specific time intervals led to this wave shape profile.

Fig. 11 shows the change of concentration with velocity at times 1, 4, and 8 days. From this figure, it is noticed that the concentrations, at downstream of the pool, increases with increasing interstitial velocity to 2.34 cm/h and then the concentration decreases to lower limit, except that at sampling points (−7.5, 20, 1) (−7.5, 20, 3) and (2.5, 20, 3). The reason may be attributed to the dispersion is dominated at velocity equal or less than 2.34 cm/h which leads to increase the concentration. While at velocity more than 2.34 cm/h, the advection is dominated which cause more dilution for the mixture of benzene and water, this will decrease the concentration in the downstream of benzene pool. At sampling points (−7.5, 20, 1), (−7.5, 20, 3), and (2.5, 20, 3); where the locations are situated under or adjacent to the benzene/water interface; the behaviors of concentration with velocity are differed than those in the other figures. The reason for these behaviors at these locations and at certain hydrodynamic and contact time conditions, the dispersive concentrations increase or decrease depending on the effect of these conditions.

When the velocity equals to 3.60 cm/h and at horizontal distance ($x$) of 62.5, all concentration profiles in Figs. 7–10 are approximately similar and increased with time. These figures have also shown the concentration profile is more stable at the farthest distance from the pool (62.5 cm).

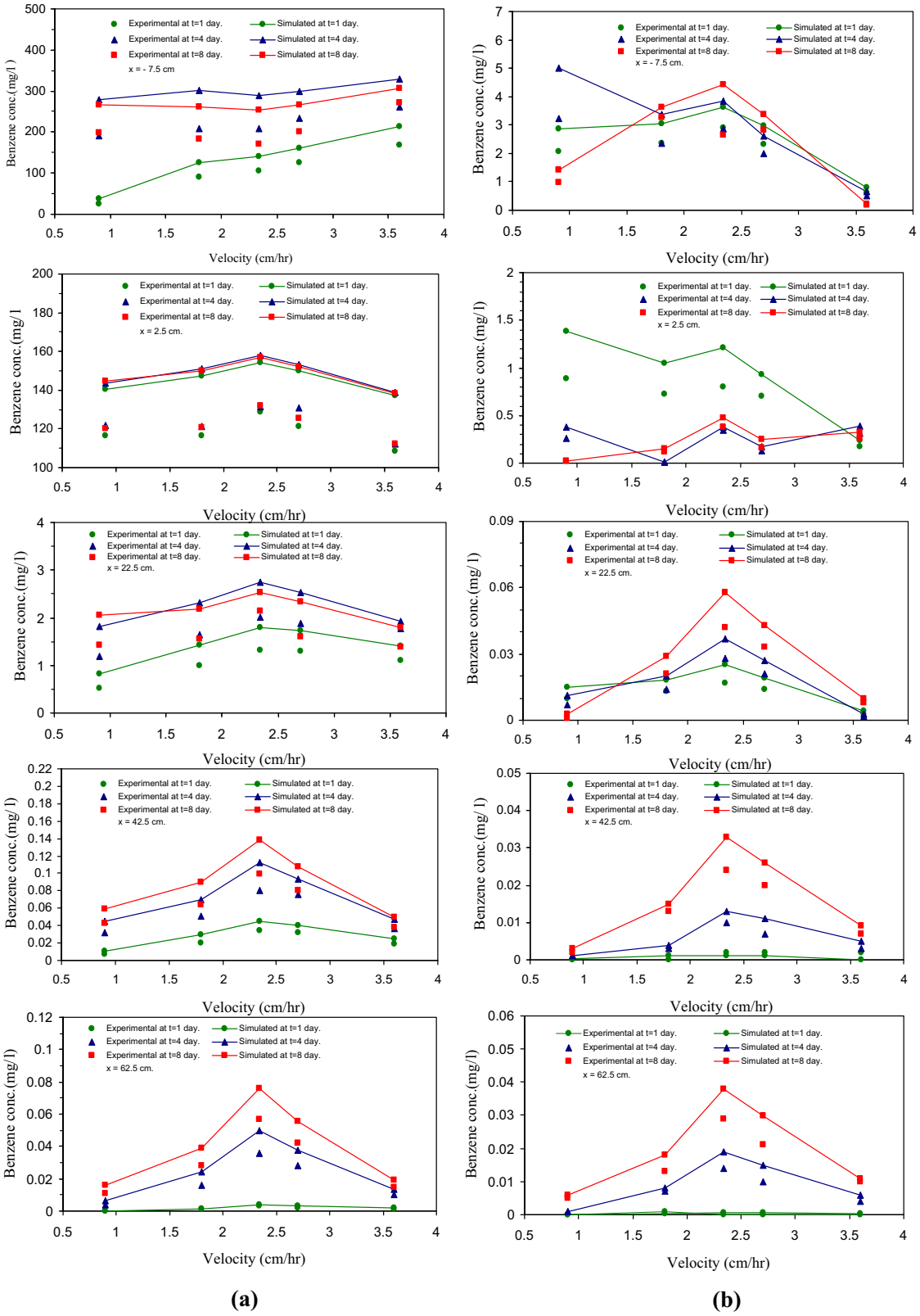


**Fig. 11.** The change of experimental and simulated benzene concentration with interstitial velocity at $y = 20$ cm and at depths (a) $z = 1$ cm; (b) $z = 3$ cm.

Fig. 12 shows the change of the measured and finite element numerical model of benzene concentrations with distance ($x$) below and downstream of the benzene pool at different sampling times, Lateral distance $y = 20$ cm, and at depths ($z$) 1 cm and 3 cm, respectively. In general, the concentration values decreased with distance. In Fig. 12(a), at depth of 1 cm, the concentration profile is sharply declined through the distance between −7.5 cm and 22.5 cm then continue to decrease with distance to lower limits. While in Fig. 12(b), at depth of 3 cm, the concentration versus distance is sharply declined through the distance −7.5 cm and 2.5 cm.

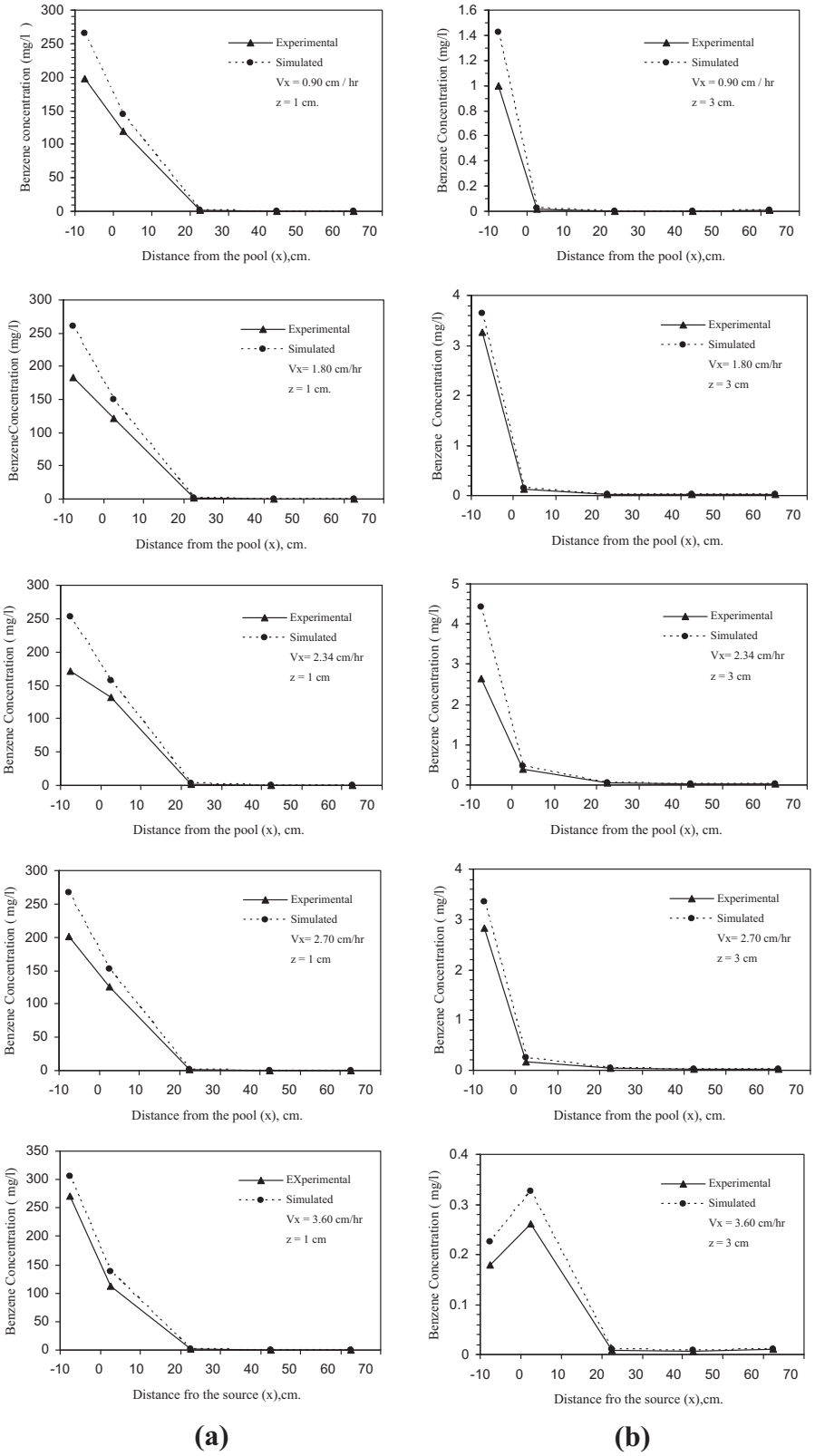


**Fig. 12.** The experimental and simulated concentrations of benzene versus distance from the pool ($x$) at different interstitial velocities, $y = 20$ cm, and depth (a) 1 cm; (b) 3 cm.

Except that at velocity of 3.60 cm/h, the behavior of concentration differs from the other figures. The concentration profile increases within the distance −7.5 cm to 2.5 cm and then sharply declines until it reaches distance of 22.5 cm. Then, it continues to decrease reaching the lower limit. At these distances, the sampling points are situated in holes $a$ and $b$; under and near the benzene pool, respectively (at $x = -7.5$ cm, $y = 20$ cm, $z = 3$ cm; and $x = 2.5$ cm, $y = 20$ cm, $z = 3$ cm).

**Table 2**
Parameters for simulation the distribution of concentration with depth $z$ [35].

| Parameter | Value |
|---|---|
| Interstitial velocity ($V_x$) | 1 m/day |
| Longitudinal dispersivity ($\alpha_x$) | 0.1 m |
| transverse dispersivity ($\alpha_y$) | 0.01 m |
| Vertical dispersivity ($\alpha_z$) | 0.01 m |
| Effective molecular diffusion coefficient ($D_e$) | $4.15 \times 10^{-5}$ m$^2$/day |

## 7. Verification and accuracy of the finite element numerical model solution

The finite element numerical model has been tested to determine its validity. The verification of this model is based on the comparison with results of the laboratory scale aquifer experiments. The comparison shows that the model results overpredict the experimental within factor 1.60 for depth of 1 cm in the porous medium, and 2.29 for depth of 3 cm.

In this paper, the regression analysis is used to find the relationship between the calculated and observed LNAPL concentration data at each sampling location and for all velocities. The regression analysis shows a good correlation between the calculated and measured concentration data. The obtained correlation coefficients are significant at 5% confidence level. The significance is sufficient to indicate that the model is operating within a reasonable limit of error.

In order to verify the developed finite element (F.E.) numerical model of the present paper, no significant data specified for benzene are available in the literature regarding dissolution in three-dimensional homogeneous, isotropic, and uniform flow in saturated porous medium. Therefore, the developed model is tested for the concentration data presented by [35]. These data are obtained from simulation of DNAPL dissolution by the numerical model using finite difference (F.D.) method. The parameters and their values used in the simulation are shown in Table 2. The verification is accomplished to find the distribution of concentration with the vertical distance ($z$), at $x = 200$ cm and $y = 550$ cm. The comparison is illustrated in Fig. 13. As shown in this figure, the finite difference (F.D.) concentration values are higher than those of the finite element (F.E.). The application or implementation of a method (finite element, finite difference) by each developed model is different from other in solving the numerical model. This can be considered as one of the reasons for the interpretation of the differences between the results of the two developed models. Furthermore, there are other reasons for this difference such as; the concentration results from the dissolution of circular pool shape of the present model are compared with those results from the dissolution of rectangular pool shape given by [35]. Also, the finite difference model depends on a general NAPL code.

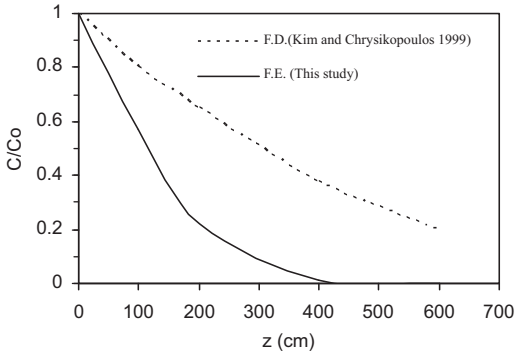


**Fig. 13.** Comparison of the finite element concentration values of the present study with those of finite difference by Kim and Chrysikopoulos [35].

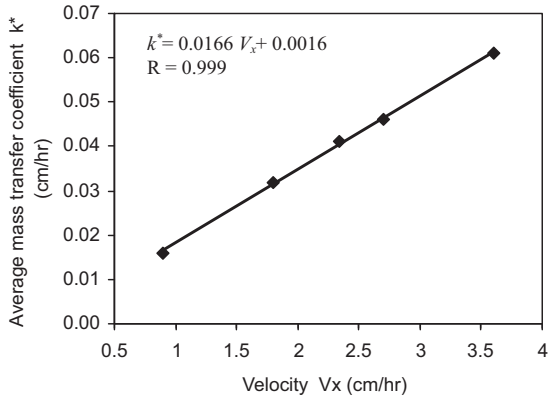


**Fig. 14.** The change of the average mass transfer coefficient ($k^*$) with the interstitial velocity ($V_x$).

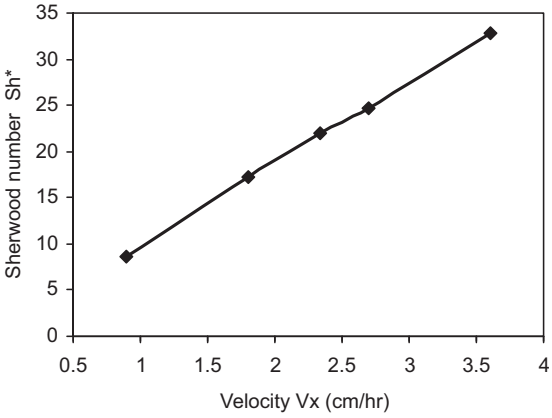


**Fig. 15.** The dimensionless mass transfer (modified Sherwood number $Sh^*_{(e)}$) behavior with the interstitial velocity ($V_x$).

In general, it is concluded that the finite element numerical results of the present paper overestimate the measured results of the laboratory scale aquifer, and underestimate those of the finite difference which presented by [35].

## 8. Correlating mass transfer behavior with hydrodynamic conditions

The concentration of a dissolved NAPL in groundwater is governed mainly by interface mass-transfer processes that are often slow and rate limited [7,36,37].

Because of the existing of equilibrium mass transfer condition at interstitial velocities of up to 4.17 cm/h [36], the interstitial velocities used for experiments and model simulations in the present study are 0.90, 1.80, 2.34, 2.70, and 3.60 cm/h.

The time invariant average mass transfer coefficient ($k^*$) is experimentally determined by using the following equation [38]:

$$k^* = n\sqrt{\frac{4D_z V_x}{\pi l_{c(e)}}} \tag{17}$$

where $l_{c(e)}$ is the characteristic length of the pool. $l_{c(e)}$ employed here is the square root of the circular pool area. Fig. 14 indicates that $k^*$ is proportional to the interstitial velocity ($V_x$). This behavior is attributed to the increasing of the concentration gradients at the NAPL–water interface with increasing $V_x$. The best fit relation to the time invariant average mass transfer coefficient ($k^*$) as a function of interstitial velocity ($V_x$) is:

$$k^* = 0.0166V_x + 0.0016 \tag{18}$$

**Table 3**
Values of $k^*$, $Sh^*_{(e)}$, $Pe^*_{x(e)}$, and $Pe^*_{y(e)}$ for different velocities ($V_x$) and hydrodynamic dispersion coefficients ($D_x$, $D_y$, and $D_z$).

| $V_x$ (cm/h) | $D_x$ (cm$^2$/h) | $D_y$ (cm$^2$/h) | $D_z$ (cm$^2$/h) | $k^*$ (cm/h) | $Pe^*_{x(e)}$ | $Pe^*_{y(e)}$ | $Sh^*_{(e)}$ |
|---|---|---|---|---|---|---|---|
| 0.90 | 0.284 | $2.84 \times 10^{-2}$ | $2.84 \times 10^{-2}$ | 0.016 | 23.73 | 237.34 | 8.66 |
| 1.80 | 0.553 | $5.53 \times 10^{-2}$ | $5.53 \times 10^{-2}$ | 0.032 | 24.40 | 244.03 | 17.22 |
| 2.34 | 0.696 | $6.96 \times 10^{-2}$ | $6.96 \times 10^{-2}$ | 0.041 | 25.22 | 252.20 | 22.06 |
| 2.70 | 0.780 | $7.80 \times 10^{-2}$ | $7.80 \times 10^{-2}$ | 0.046 | 25.96 | 259.60 | 24.75 |
| 3.60 | 1.014 | $1.014 \times 10^{-1}$ | $1.014 \times 10^{-1}$ | 0.061 | 26.63 | 266.30 | 32.82 |

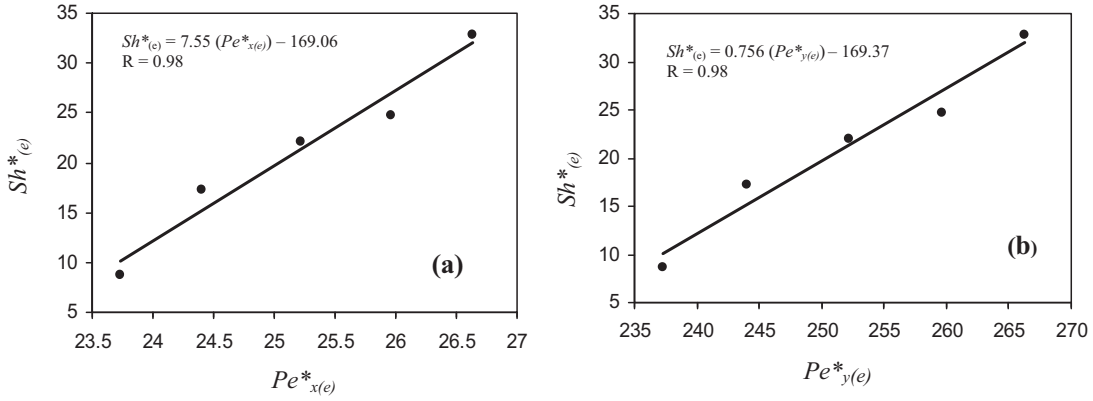


**Fig. 16.** Best fit relationship between the experimentally determined overall mass transfer and (a) $Pe^*_{x(e)}$; (b) $Pe^*_{y(e)}$.

The dimensionless mass transfer behavior is summarized in terms of the modified Sherwood number, $Sh^*_{(e)} = k^* \cdot l_{c(e)}/D_e$, where $D_e = D_m/\tau$ is the effective molecular diffusion coefficient in the porous medium (where $D_m$ is the molecular diffusion coefficient and $\tau \geq 1$ is the tortuosity coefficient). The computed $l_{c(e)}$, and $D_e$ for the present paper are 13.29 cm and $2.47 \times 10^{-2}$ cm$^2$/h, respectively. Fig. 15 illustrates the linear relationship between the Sherwood number and the interstitial velocity.

The average Peclet numbers, $Pe^*_{x(e)}$, and $Pe^*_{y(e)}$ represent the advective–dispersive mass transfer in $x$ and $y$ directions for circular pool, respectively. They are obtained by using the following equations:

$$Pe^*_{x(e)} = \frac{V_x r}{D_x} \tag{19}$$

$$Pe^*_{y(e)} = \frac{V_x r}{D_y} \tag{20}$$

where $r$ is the radius o f LNAPL pool. Table 3 shows the determined $k^*$, $Sh^*_{(e)}$, $Pe^*_{x(e)}$, and $Pe^*_{y(e)}$ for all velocities ($V_x$) and the hydrodynamic dispersion coefficients ($D_x$, $D_y$, $D_z$).

To find the correlations between the time invariant Sherwood number and overall Peclet numbers; $Pe^*_{x(e)}$ and $Pe^*_{y(e)}$ separately, statistica program is used to fit the experimental data (Table 3). The correlations which give the best fitting and greater correlation coefficient ($R$) are linear correlations (Fig. 16). The overall Sherwood number correlations found in the present study are:

$$Sh^*_{(e)} = 7.55(Pe^*_{x(e)}) - 169.06 \tag{21}$$

$$Sh^*_{(e)} = 0.756(Pe^*_{y(e)}) - 169.37 \tag{22}$$

The correlation coefficients ($R$) for these fittings are equal to 0.98. Eqs. (21) and (22) are applicable to circular LNAPL pool dissolution in three-dimensional, homogeneous, uniform flow, and saturated porous medium.

## 9. Conclusions

This research reaches to the following conclusions based on the analysis of the results of both experimental and numerical investigations. The concentration profile sharply declines at the horizontal distances which are nearest to the source and then continues to decrease with increasing distance to the lower values. In spite of the experimental concentrations are not very close with the corresponding numerical model concentrations but the same behavior with time and distance are obtained. The comparison shows that the model results overpredict the experimental ones within factor 1.60 at depth of 1 cm in the porous medium, and 2.29 at depth of 3 cm. The results of the statistical analysis of the experimental and numerical have shown the regression analysis for both experimental and calculated results give the values of correlation coefficients ranged between 0.8485 and 0.9986. Good agreement is shown between the experimental results and the simulated concentration profiles.

The time invariant average mass transfer coefficient is found at different interstitial velocities. The values of this coefficient are ranged from 0.016 to 0.061 cm/h. It is increased proportionally with velocity toward a limiting value. Parameter estimates for $Pe^*_{x(e)}$, $Pe^*_{y(e)}$, $Sh^*_{(e)}$ are determined at different hydrodynamic conditions.

## References

[1] G.S. Moore, J.H. Villenave, J.C. Hickey, Characterization of petroleum contaminants in ground-water and soils, in: P. Kostecki, E. Calabrese, M. Bonazountas (Eds.), Hydrocarbon Contaminated Soil, Chelsea Lewis Publishers, USA, 1992.
[2] K. Hiscock, Ground-water pollution and protection, in: O'Riordan (Ed.), Environmental Science for Environmental Management, 1995.
[3] P. Makri, D.K. Kalivas, G. Bathrellos, H. Skilodimou, Spatio-temporal analysis of ground-water pollution from BTEX in Thriassio Field-Attica-Greece, IAEG, no. 409, 2006.
[4] C.J. Newell, S.D. Acree, R.R. Ross, S.G. Huling, Light nonaqueous phase liquids, EPA Ground Water Issue, EPA/540/S-95/500, September 1995.
[5] T.S. Phophi, The occurrence and evaluation of LNAPLs contamination in urban areas of South Africa, Master thesis, University of the Free State, Bloemfontein, South Africa, 2004.
[6] J.S. Christensen, J. Elton, Soil and Ground-water Pollution from BTEX, 2005, www.cee.vt.edu/prorgram_areas/environmental/teach/gwprimer/btex/btex.html.

[7] D.M. Mackay, P.V. Roberts, J.A. Cherry, Transport of organic contaminants in ground-water: distribution and fate of chemicals in sand and gravel aquifers, Environ. Sci. Technol. 19 (5) (1985) 384–392.
[8] K.Y. Lee, C.V. Chrysikopoulos, Numerical modeling of three-dimensional contaminant migration from dissolution of multicomponent NAPL pools in saturated porous media, Environ. Geol. 26 (3) (1995) 157–165.
[9] C.V. Chrysikopoulos, P.-Y. Hsuan, M.M. Fyrillas, Bootstrap estimation of the mass transfer coefficient of a dissolving nonaqueous phase liquid pool in porous media, Water Resour. Res. 38 (3) (2002).
[10] B.K. Dela Barre, T.C. Harmon, C.V. Chrysikopoulos, Measuring and modeling the dissolution of nonideally shaped dense nonaqueous phase liquid pools in saturated porous media, Water Resour. Res. 38 (8) (2002).
[11] K.Y. Lee, C.V. Chrysikopoulos, Dissolution of a well-defined trichloroethylene pool in saturated porous media: experimental results and model simulations, Water Res. 36 (2002) 3911–3918.
[12] W.M.J. Bao, E.T. Vogler, C.V. Chrysikopoulos, Nonaqueous liquid pool dissolution in three-dimensional heterogeneous subsurface formations, Environ. Geol. 43 (2003) 968–977.
[13] T.P. Clement, Y.C. Kim, T.R. Gautam, K.K. Lee, Experimental and numerical investigation of DNAPL dissolution process in a laboratory aquifer model, Ground Water Monitor. Remed. 24 (4) (2004) 88–96.
[14] K.Y. Lee, C.V. Chrysikopoulos, Dissolution of a multicomponent DNAPL pool in an experimental aquifer, Hazard. Mater. B128 (2006) 218–226.
[15] H.A. Gzar, Experimental investigation and numerical modeling of benzene dissolution and transport in a saturated zone of the soil, Ph.D. dissertation, College of Engineering/University of Baghdad, Iraq, 2010.
[16] A.E. Pearce, E.A. Voudrias, M.P. Whelan, Dissolution of TCE and TCA pools in saturated subsurface systems, Environ. Eng. 120 (5) (1994) 1191–1206.
[17] R.J. Blackwell, Laboratory studies of microscopic dispersion phenomena, Soc. Petrol. Eng. (1962) 69–76.
[18] J.C. Bruch, Two-dimensional dispersion experiments in a porous medium, Water Resour. Res. 6 (3) (1970) 791–800.
[19] H.E. Kobus, K. Spitz, Transverse mixing of stratified flows in porous media, in: Presented at the 21st Congress of International Association for Hydraulic Research, Melbourne, Australia, August 19–23, 1985, pp. 169–174.
[20] E.A. Sudicky, R.W. Gillham, E.O. Frind, Experimental investigation of solute transport in stratified porous media. I. The nonreactive case, Water Resour. Res. 21 (7) (1985) 1035–1041.
[21] G.A. Robbins, Methods for determination of transverse dispersion coefficient of porous media in column experiment, Water Resour. Res. 25 (6) (1989) 1249–1258.
[22] C.V. Chrysikopoulos, Three-dimensional analytical models of contaminant transport from nonaqueous phase liquid pool dissolution in saturated subsurface formation, Water Resour. Res. 31 (4) (1995) 1137–1145.
[23] C.V. Chrysikopoulos, T.-J. Kim, Local mass transfer correlations for nonaqueous phase liquid pool dissolution in saturated porous media, Transport Porous Media 38 (2000) 167–187.
[24] I.M. Smith, D.V. Griffiths, Programming The Finite Element Method, John Wiley Sons, 1998.
[25] J.E. Bowles, Engineering Properties of Soils and their Measurement, McGraw-Hill Kogakusha, Ltd., 1978.
[26] A.W. Al-Khafaji, O.B. Andersland, Geotechnical Engineering and Soil Testing, Saunders College Publishing, 1992.
[27] C.V. Chrysikopoulos, K.Y. Lee, T.C. Harmon, Dissolution of a well-defined trichloroethylene pool in saturated porous media: experimental design and aquifer characterization, Water Resour. Res. 36 (7) (2000) 1687–1696.
[28] T.K. Perkins, Johnston, A review of diffusion and dispersion in porous media, Soc. Petrol. Eng. (1963) 70–81.
[29] G. de, Marsily, Quantitative Hydrogeology—Groundwater Hydrology for Engineers, Academic Press, San Diego, CA, 1981.
[30] R.J. Watts, Hazardous Wastes: Sources – Pathways – Receptors, John Willy & Sons, Inc., 1998.
[31] R.P. Schwarzenbach, J. Westall, Transport of nonpolar organic compounds from surface water to ground water, Lab. Stud. Environ. Sci. Technol. 15 (1981) 1300–1367.
[32] P.A. Domenico, F.W. Scbwartz, Physical and Chemical Hydrology, John Wiley & Sons, Inc., 1990.
[33] R.A. Griffin, W.R. Roy, Interaction of Organic Solvents with Saturated Soil–Water Systems, Environmental Institute for Waste Management Studies, The University of Alabama, Open-File Report No. 3, 1985, p. 86.
[34] American Petroleum Institute (API), Laboratory Study on Solubilities of Petroleum Hydrocarbons in Groundwater, API Publication No. 4395, 1985.
[35] T.-J. Kim, C.V. Chrysikopoulos, Mass transfer correlations for nonaqueous phase liquid pool dissolution in saturated porous media, Water Resour. Res. 35 (1999) 449–459.
[36] S.E. Powers, C.O. Loureiro, L.M. Abriola, W.J. Weber Jr., Theoretical study of the significance of nonequilibrium dissolution of nonaqueous phase liquids in subsurface systems, Water Resour. Res. 27 (4) (1991) 463–477.
[37] C.V. Chrysikopoulos, Nonaqueous phase liquid pool dissolution in subsurface formations, in: Handbook Environ. Chem., vol. 5, Part F, vol. 3, 2005, pp. 97–132.
[38] S.E. Power, S.E. Heermann, Potential ground and surface water impacts, appendix B: modeling interface mass-transfer processes, in: G. Cannon, D. Rice (Eds.), Presented in "A critical review: the effect of ethanol in gasoline on the fate and transport of BTEX in the subsurface", UCRL-AR-135949, vol. 4, Chapter 2, 1999.